Absorption enhancement by phase gradient metamaterial

Zhang Ze, Elke Deckers, Claus Claeys, Hervé Denayer, Wim Desmet

ABSORPTION ENHANCEMENT BY PHASE GRADIENT METAMATERIAL

Ze Zhang[1,3] **Elke Deckers**[2,3] **Claus Claeys**[1,3] **Hervé Denayer**[1,3] **Wim Desmet**[1,3]

[1] KU Leuven, Department of Mechanical Engineering,
Celestijnenlaan 300, 3001 Leuven, Belgium
[2] KU Leuven, Campus Diepenbeek, Department of Mechanical Engineering,
Wetenschapspark 28, 3590 Diepenbeek, Belgium
[3] DMMS lab, Flanders Make, Belgium

ze.zhang@kuleuven.be

ABSTRACT

This paper presents a design methodology to achieve enhanced absorption based on conventional porous material over a wide range of frequency and angle of incidence. Using the methodology, a metamaterial structure is designed which forms a phase gradient on both the reflected and transmitted surfaces. As governed by the generalized Snell's law, the absorbing capability is substantially enhanced by forcing all higher order modes of reflection and transmission to be evanescent. Firstly, an analytical model to predict the phase response of reflection and transmission on single cell level is derived and validated numerically. Secondly, using this model, a metamaterial structure is designed based on conventional porous material, the acoustic performance of which is then numerically validated. Lastly, samples are fabricated and the acoustic performance is validated experimentally. A substantial absorption enhancement over a foam of the same type and dimensions is found and a good match between simulation and experiment is observed.

1. INTRODUCTION

Passive noise abatement solutions can be categorized into two groups: resonance-based solutions [1–4] and non-resonance-based solutions [5, 6]. Resonance-based solutions, regardless of the specific mechanism to create the resonance, only perform well in a narrow frequency band. Multiple resonators can be assembled together to broaden this frequency band [7], however, such designs tend to be complex and cannot easily be manufactured. Non-resonance-based solutions typically involve a porous material, which exhibits a broadband characteristic. However, the ratio of absorption over thickness is low in the low to mid-frequency range.

Aiming to solve this issue, this paper presents a method of arranging porous material to form a metamaterial (section 3) using the generalized Snell's law (section 2). Favorable results of absorption are observed from both numerical prediction (section 4) and experimental validation (section 5).

2. GENERALIZED SNELL'S LAW

When acoustic waves impinge on the interface between two media, reflection and transmission will occur. If a phase discontinuity of reflection or transmission exists on the interface, multiple orders of reflection and transmission will be induced, as presented schematically in Figure 1.

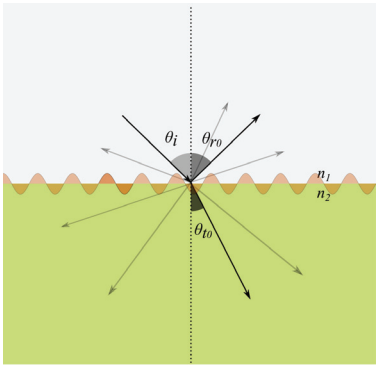

Figure 1: Schematic representation of reflection and transmission law with a PG

The higher order reflection and transmission possess different angles as compared with their counterparts which follow the conventional reflection and Snell's law. The thick black lines represent the incoming wave and reflection and transmission that follow the conventional law of reflection and Snell's law. The gray lines represent the higher orders of reflection and transmission due to the periodicity induced by the phase discontinuity. θ_i is the angle of incidence whereas θ_{r0} and θ_{t0} are the angle of reflection and transmission that follow the conventional laws. n_1 and $_2$ are the refractive indices of medium 1 and 2.

As derived in [8], the GSL states that:

$$\sin(\theta)\, n - \sin(\theta_i)\, n_1 = m\frac{\lambda_1}{2\pi}\frac{d\Phi}{ds}, \qquad (1)$$

where $\frac{d\Phi}{ds}$ is the phase gradient (PG) of the reflection or transmission coefficients on the interface, s is the distance between two points on the interface, λ_1 is the wavelength in medium 1 at frequency f, m is an integer number that

represents the different orders induced by the PG, θ is angle of reflection or transmission and n is the refractive index of medium 1 or 2. Equation (1) describes both reflection and transmission, where, as shown in Figure 1, in case of transmission, θ is θ_t (angle of transmission) and n is n_2; whereas in case of reflection, θ is θ_r (angle of reflection) and n is n_1.

The angle of reflection or transmission can be calculated by equation (1) as:

$$\theta = \text{asin}\left(\frac{1}{n}\left(\sin\left(\theta_i\right) n_1 + m\frac{\lambda_1}{2\pi}\frac{d\Phi}{ds}\right)\right). \quad (2)$$

It can be seen that different PGs and orders lead to different θ, out of which, some combinations would not yield a complex θ. It is worth noting that by setting the PG to zero, the GSL is reduced to the conventional law of reflection and Snell's law. From equation (2), one can also conclude that if $|\frac{d\Phi}{ds}| > \frac{2\pi}{\lambda_1}(n+n_1)$ and for $|m| \geq 1$, the reflection or transmission angle θ will have a complex solution irregardless of value of θ_i. This means that the wavenumbers of all higher order modes are complex numbers with a purely imaginary component in the direction normal to the interface. Hence, with a sufficiently large PG, all higher order modes of reflection or transmission can be converted into evanescent waves depending on the interface where the PG is applied.

Consequently, if a sufficiently large PG is applied on both the reflection and transmission interfaces, then the propagation of both the higher orders of reflection and transmission in the direction normal to the interface can be suppressed. Study shows that when a PG exists, the majority of the energy goes to the higher order modes [9]. As a result, the suppression of the higher order modes leads to a substantial absorption enhancement.

3. THE METAMATERIAL DESIGN

A design that generates PGs on both the reflection and transmission surfaces is introduced in this section. Practically, discrete cells are used to induce the two PGs. Thus, it is favorable that each cell possesses the capability to adjust the two PGs independently, which means the cell design should possess two degrees of freedom (DoFs) once the outer dimensions are determined. As shown in figure 2, each cell is a stacking of an air, porous and air layers together, which serves the need.

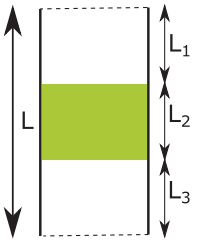

Figure 2: Schematic representation of one cell of the design, the white regions represent air layers and the green region represents the porous layer

The two DoFs for each cell are location and the thickness of the porous material or the thickness of the air layer above and below the porous material. Thus, by varying these variables the phase of reflection and transmission can be adjusted at a greater flexibility.

For a design of this kind, the reflection and transmission coefficients can be calculated analytically by solving the pressure field of different layers considering the continuity of acoustic particle velocity and pressure at the interfaces. The transmission coefficient (T) and reflection coefficient (R) are expressed as:

$$T = \frac{e^{k_0(L_1+L_3)j} 2Z_0Z_1}{\left(Z_0^2+Z_1^2\right) j\sin\left(k_1L_2\right) + 2Z_0Z_1\cos\left(k_1L_2\right)} \quad (3)$$

and

$$R = \frac{-e^{-2k_0(L_1+L_2)j}\left(Z_0^2-Z_1^2\right) j\sin\left(k_1L_2\right)}{\left(Z_0^2+Z_1^2\right) j\sin\left(k_1L_2\right) + 2Z_0Z_1\cos\left(k_1L_2\right)}, \quad (4)$$

where k_0, k_1, Z_0 and Z_1 are acoustic wavenumber and characteristic impedance of air and foam, respectively.

To validate the phase model, single cell level simulations are made in COMSOL using the pressure acoustics module, where the phase of R and T are extracted. Two unique cells are evaluated. Table 1 shows a comparison of predicted phase using equation 3 and 4 and those directly extracted from the simulation, where a good match can be found.

Case	R (°)		T (°)	
	Analytical	Numerical	Analytical	Numerical
1	101.7	102.4	-161.4	-161.5
2	-62.8	-63.7	67.4	67.9

Table 1: Phase of R and T: analytical vs numerical

A lightweight melamine foam is chosen as the porous layer. The complex frequency-dependent wavenumber and characteristic impedance of the material are obtained from an impedance tube measurement using two cavity method [10]. Figure 3 shows the retrieved parameters.

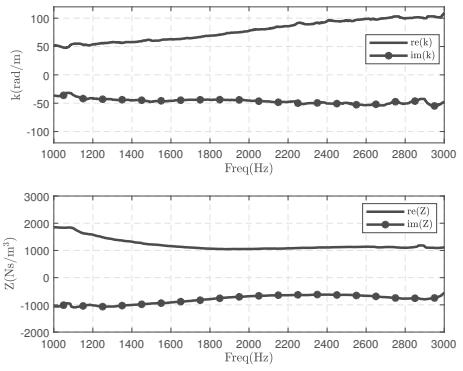

Figure 3: Retrieved equivalent wavenumber k and impedance Z of the samples

Equation (3) and (4) are then used to predict the phase of reflection and transmission coefficients of a cell with

varying air layer thickness at 2000 Hz. The phase of reflection and transmission are shown in figure 4 and 5 for a 7 cm L. For a fixed L, one can see that the phase of T is solely dependent on the thickness of the porous layer L_2. The dependency of the phase of R can be divided into two regions: the thick foam region and the thin foam region. In the former region, the phase of R is mainly dependent on L_1; whereas in the latter region, it depends on both L_1 and L_2.

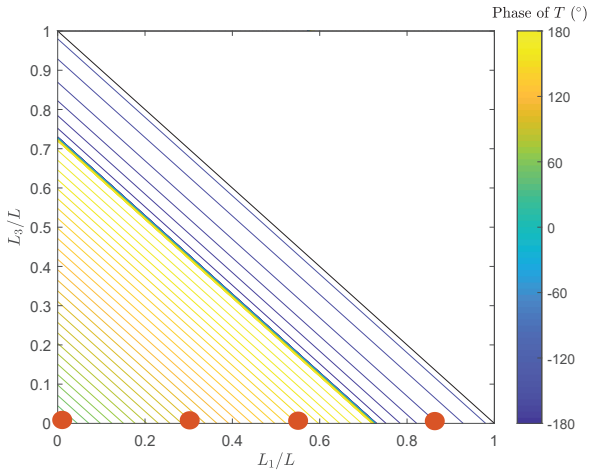

Figure 4: Phase of T as a function of L_1 and L_3 at 2000 Hz

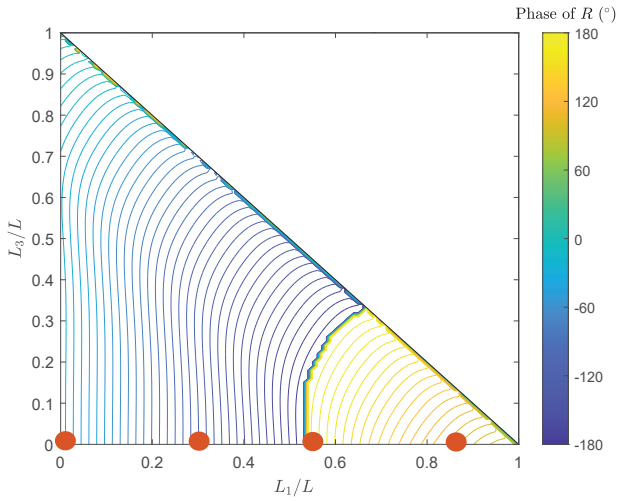

Figure 5: Phase of R as a function L_1 and L_3 at 2000 Hz

Based on the figures, four cells of different air layer thickness are chosen and placed side by side to form a PG on both reflection and transmission interface, shown as the orange circles in Figure 4 and 5. A schematic representation is shown in figure 6.

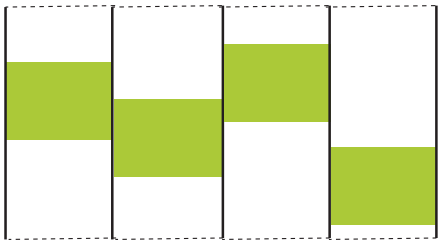

Figure 6: Schematic representation of a period composing of four cells

4. NUMERICAL PREDICTIONS

The absorbing performance of the proposed metamaterial is predicted using commercial software COMSOL Multiphysics 5.5. The pressure acoustics module is used, which solves the Helmholtz equation in the domain. For more details of the numerical setup and numerical results, please refer to [9]. Figure 7 shows a schematic representation of the numerical model.

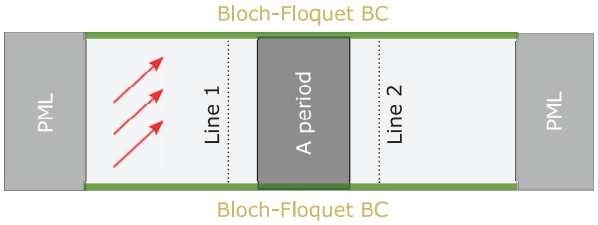

Figure 7: Schematic representation of the numerical model

A period of four cells are placed in the middle of the acoustic domain. Two perfectly matched layers (PMLs) are added to two ends of the domain, suppressing the reflections from the boundaries back to the sample. On two sides, Bloch-Floquet boundary conditions are applied, which simulate the metamaterial of infinite extent with each period right next to each other. The foam region is described as equivalent fluid using the characterized parameters. A plane wave incident field with a controlled angle of incidence and amplitude is applied to the acoustic domain on the left hand side of the sample. A mixture of quad and triangle meshes are used with a maximum size not exceeding $\frac{1}{20}$ of the smallest wavelength in the frequency range, which is 1000 Hz to 3000 Hz with a 20 Hz increment. The pressure of the reflected field and the transmitted field is extracted on two lines that are 10 cm from the cell surface. The following relations are used to obtain R and T:

$$R = \frac{P_{s,l_1}}{P_i}, \tag{5}$$

$$T = \frac{P_{t,l_2}}{P_i}, \tag{6}$$

$$\alpha = 1 - R^2 - T^2, \tag{7}$$

where l_1 and l_2 are two parallel lines 10 cm from the surface of the cells, P_i is the amplitude of the incidence field, $P_{s,l}$ is the algebraic average of pressure amplitude of the

scattered field on line l, $P_{t,l}$ is the algebraic average of pressure amplitude of the total field on line l.

For comparison, a porous material of the same material properties and outer dimensions as the metamaterial is simulated with the same numerical setup. Figure 8 shows the absorption coefficients of the metamaterial and the porous material at normal incidence.

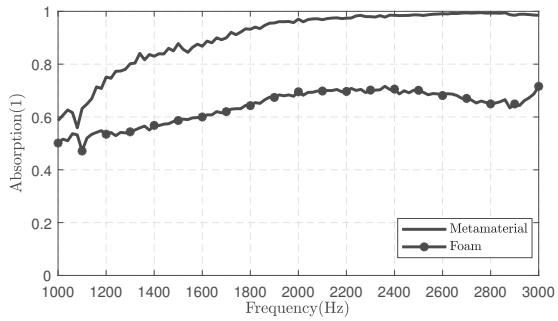

Figure 8: Absorption coefficient α of metamaterial and benchmark foam at normal incidence

A substantial absorption enhancement can be observed between 1000 Hz and 3000 Hz for the normal incidence case for the metamaterial. The peak and dip from 1000 Hz to 1100 Hz for both cases and the upward curve shape for the porous material around 3000 Hz are possibly due to the imperfect characterized material parameters from experiment as similar peaks and dips can be observed for other materials inside the same impedance tube.

To study the acoustic performance of the proposed metamaterial under oblique incidences, the acoustic performance of the design is further predicted numerically under various oblique angles of incidences. The results are shown in figure 9.

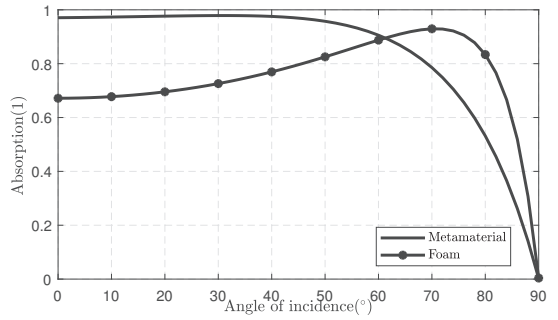

Figure 9: Angle-dependent absorption coefficient α of metamaterial and benchmark foam at 2000 Hz

Rather different absorption coefficient curve shapes are observed for two cases. For the proposed metamaterial, a wide high absorption region is located around the normal incidence; whereas the absorption of the foam peaks at an angle of incidence around 70°. Besides the fact that the high absorption region is wider for the metamaterial, the high absorption for smaller angles of incidence is advantageous for many applications. In a typical diffuse field calculation, angles of incidence above 78° are omitted since the energy components from these angles are minimal [11].

It can be concluded that, compared with a porous material of the same thickness, the metamaterial has a better absorbing behavior both for normal and diffuse field excitation.

5. EXPERIMENTAL VALIDATION

A metamaterial sample consisting of nine periods as shown in Figure 10 is manufactured. The rigid partitions in the design are realized by aluminum plates of 3 mm thick. Given a large discrepancy of acoustic impedance between foam and aluminum and between air and aluminum, the aluminum plates are expected to behave as rigid partitions. The porous samples are manufactured using a hot wire cutter. The aluminum plates are manufactured by a stamping press.

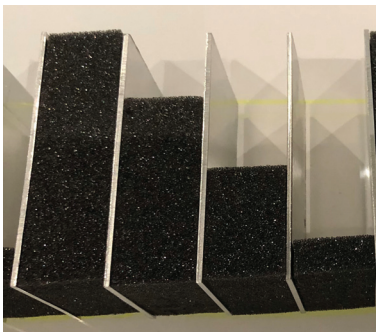

Figure 10: A manufactured period of samples

The samples are measured in a 2D impedance tube designed, manufactured and validated at KU Leuven [12], which is capable of measuring angle-dependent reflection, transmission and absorption coefficients over a frequency range based on the modal decomposition method. Based on the measured scattering matrix of the system, the absorption coefficient of each duct mode and the absorption coefficient at a specific angle of incidence can be obtained. Figure 11 shows the 2D impedance tube with the sample inside.

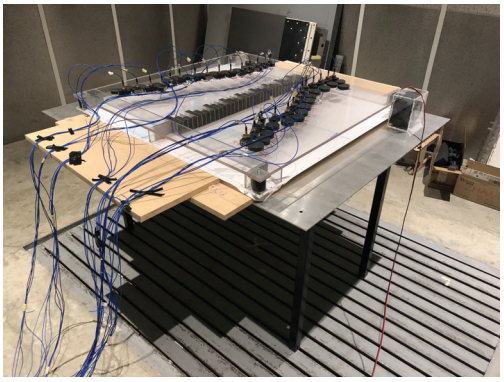

Figure 11: The experimental setup

For details of the experimental setup, please refer to [9]. A summary of the setup is listed in Table 2.

Signal acquisition system	Simcenter SCADAS
Excitation signal	Broadband white noise
Quality considered	FRF
Sampling frequency	16384 Hz
Number of averages for FRF	100
Number of measuring points	60
Microphone type	PCB type 378C10
Sound source type	Monacor KU-516
Number of measurements	32

Table 2: Experiment setup details

Each measurement is conducted with a specific sound source location. Given the limited number of available microphones, for each source location, the samples are measured twice to cover all microphone locations. The two sub-measurements are subsequently merged in the post-processing.

The normal incidence absorption for the metamaterial from the measurement and from the numerical prediction are shown in figure 12.

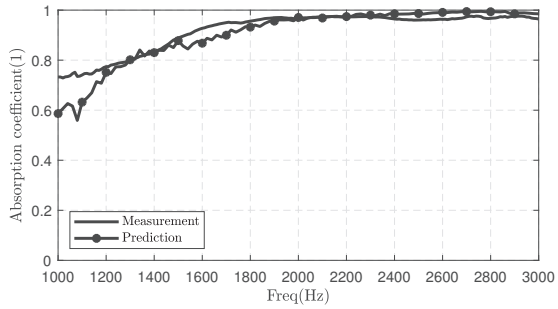

Figure 12: Absorption coefficient of the metamaterial at normal incidence from the measurement and numerical prediction

A good agreement can be observed, which indicates that the metamaterial works as intended. The slight mismatch between 1000 Hz to 1200 Hz is possibly due to the inaccurate material characterization of the porous material.

The absorption coefficient curves at oblique incidences are shown in figure 13, where a good match can also be observed.

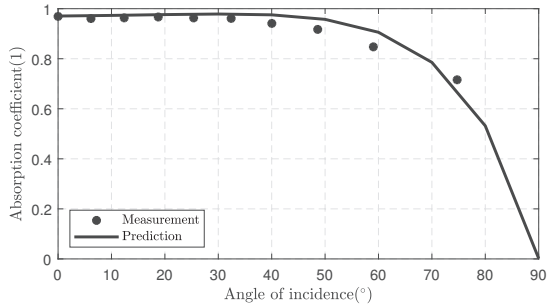

Figure 13: Absorption coefficient of the metamaterial at oblique incidence at 2000 Hz from the measurement and numerical prediction

Contrary to the rather fine resolution absorption curve from the simulation, several discrete points are obtained from the experiment, which is due to the limitation of the measurement method, i.e., only absorption coefficient at an angle of incidence that corresponds to a mode can be obtained.

6. IMPEDANCE ANALYSIS

To gain more insights into the absorption enhancement mechanism, each of the four cells with dimensions used in experiments is simulated separately to obtain the surface impedance of each cell. The setup is similar to the one in section 4, with the complete period replaced by a certain cell of a period. The linear average of acoustic pressure P_i and acoustic particle velocity v_i on the left surface of sample i (incidence side) are obtained from the simulation. The surface impedance Z_i of cell i is calculated as:

$$Z_i = \frac{P_i}{v_i}. \tag{8}$$

The simulation is performed from 1000 Hz to 3500 Hz.

Figure 14 shows the polar plot of complex surface impedance of four cells from each simulation.

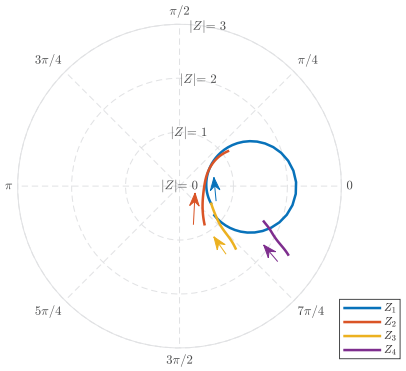

Figure 14: Polar plot of complex surface impedance under normal incidence of four cells

The arrows indicate the direction of the curve progression from 1000 Hz to 3500 Hz. A big variation of surface impedance is observed among the four samples.

To study the influence of the PG (i.e., once four samples are combined) on the absorption enhancement, the surface impedance of a period is also obtained in the simulation, which is denoted as Z_{sn}. Besides, at normal incidence, a period is regarded as a parallel assembly of four samples, with the surface impedance of a period being approximated as:

$$Z_{sc} = \frac{4}{\frac{1}{Z_1} + \frac{1}{Z_2} + \frac{1}{Z_3} + \frac{1}{Z_4}}. \tag{9}$$

The polar plot of complex impedance Z_{sn} and Z_{sc} are shown in figure 15.

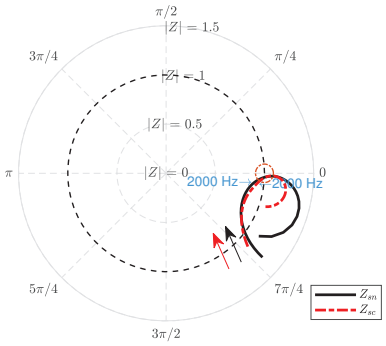

Figure 15: Polar plot of complex surface impedance of a period under normal incidence extracted directly from the simulation and calculated based on parallel assembly

Two observations can be made from the comparison. Firstly, a considerable mismatch between the two curves are observed. This is due to the fact that the period length is comparable to the wavelength within the frequency range, which means the period can no longer be regarded as sub-wavelength and parallel assembly is no longer valid.

Secondly, the design frequency (2000 Hz) is very close to the surface impedance perfect matching point as illustrated by the dashed orange circle. This means that PG induces a (quasi-)perfect matching condition on the metamaterial surface around the design frequency.

7. CONCLUSIONS

In this paper, a metamaterial based on lightweight melamine foam and GSL is proposed. It is numerically predicted and experimentally validated that absorption enhancement can be achieved by the metamaterial for normal and oblique incidence scenarios compared with a porous material of the same material properties and outer dimensions. Based on a numerical impedance analysis, it is shown that the parallel assembly of impedance no longer holds in this case due to the above sub-wavelength period length. Further, the absorption enhancement is believed to be caused by the (quasi-)perfect matching condition induced by the PG.

8. REFERENCES

[1] L. Schwan, O. Umnova, and C. Boutin, "Sound absorption and reflection from a resonant metasurface: Homogenisation model with experimental validation," *Wave Motion*, vol. 72, pp. 154–172, 2017.

[2] V. Romero-García, G. Theocharis, O. Richoux, A. Merkel, V. Tournat, and V. Pagneux, "Perfect and broadband acoustic absorption by critically coupled sub-wavelength resonators," *Scientific reports*, vol. 6, p. 19519, 2016.

[3] M. Yang, C. Meng, C. Fu, Y. Li, Z. Yang, and P. Sheng, "Subwavelength total acoustic absorption with degenerate resonators," *Applied Physics Letters*, vol. 107, no. 10, p. 104104, 2015.

[4] J.-P. Groby, R. Pommier, and Y. Aurégan, "Use of slow sound to design perfect and broadband passive sound absorbing materials," *The Journal of the Acoustical Society of America*, vol. 139, no. 4, pp. 1660–1671, 2016.

[5] A. Elliott, R. Venegas, J. Groby, and O. Umnova, "Omnidirectional acoustic absorber with a porous core and a metamaterial matching layer," *Journal of Applied Physics*, vol. 115, no. 20, p. 204902, 2014.

[6] A. Azbaid El Ouahabi, V. V. Krylov, and D. J. O'Boy, "Quasi-flat acoustic absorber enhanced by metamaterials," in *Proceedings of Meetings on Acoustics 168ASA*, vol. 22, p. 040002, Acoustical Society of America, 2014.

[7] N. Jiménez, J.-P. Groby, V. Pagneux, and V. Romero-García, "Iridescent perfect absorption in critically-coupled acoustic metamaterials using the transfer matrix method," *Applied Sciences*, vol. 7, no. 6, p. 618, 2017.

[8] N. Yu, P. Genevet, M. A. Kats, F. Aieta, J.-P. Tetienne, F. Capasso, and Z. Gaburro, "Light propagation with phase discontinuities: generalized laws of reflection and refraction," *science*, vol. 334, no. 6054, pp. 333–337, 2011.

[9] Z. Zhang, C. Claeys, H. Denayer, W. Desmet, and E. Deckers, "Design, analysis and experimental validation of a gradient-based acoustic metasurface for broadband, wide angle of incidence absorption enhancement," *Submitted to Journal of Mechanical Systems and Signal Processing*.

[10] Z. Zhang, E. Deckers, C. Claeys, and W. Desmet, "Broadband, wide angle of incidence sound absorption enhancement using rigid-backing-free periodic composite structure via wave manipulation," in *Proceedings of ISMA2020-USD2020*, 2020.

[11] H.-J. Kang, J.-G. Ih, J.-S. Kim, and H.-S. Kim, "Prediction of sound transmission loss through multilayered panels by using gaussian distribution of directional incident energy," *The Journal of the Acoustical Society of America*, vol. 107, no. 3, pp. 1413–1420, 2000.

[12] Z. Zhang, H. Denayer, C. Claeys, W. Desmet, and E. Deckers, "Angle-dependent reflection, transmission and absorption coefficients measurement using a 2d waveguide," *Submitted to Applied Acoustics*.